metals

MDPI

Article

Maximising the Deposition Rate of 5356 Aluminium Alloy by CMT-Twin-Based WAAM While Reducing Segregation-Related Problems by Local IR Thermography

Lexuri Vazquez *, Amaia Iturrioz, Pablo Lopez de Uralde and Pedro Alvarez

LORTEK Technological Centre, Basque Research and Technology Alliance (BRTA), 20240 Ordizia, Spain; aiturrioz@lortek.es (A.I.); palvarez@lortek.es (P.A.)
* Correspondence: lvazquez@lortek.es

Abstract: The CMT-Twin-based wire and arc additive manufacturing (WAAM) process for 5356 aluminium alloy has been investigated focusing on the optimisation of welding parameters to maximise the deposition rate while avoiding segregation-related problems during solidification. For that, different conditions have been studied regarding interpass dwell time and the use of forced cooling. The larger heat input produced by the double-wire CMT-Twin process, compared to the single-wire CMT, creates vast segregations for less intensive cooling conditions and short dwell times that can induce cracks and reduce ductility. Thermography has been applied to set a maximum local temperature between consecutive layers avoiding those segregations and pores, and to optimise the total manufacturing time by varying the interpass dwell time along the height of the wall. Only a constant interpass long dwell time of 240 s and the new optimised strategy were effective in avoiding merged segregations, reducing the latest total manufacturing time by 36%. Obtained tensile properties are comparable to other works using WAAM for this alloy, showing lower properties in the vertical orientation. The use of CMT-Twin-based welding technology together with variable interpass dwell time controlled by thermography is an interesting alternative to build up parts with wall thicknesses around of 10 mm in a reduced time.

Keywords: WAAM; 5356 aluminium alloy; deposition rate; CMT-Twin; interpass dwell time; cracking; segregations

check for updates

Citation: Vazquez, L.; Iturrioz, A.; Lopez de Uralde, P.; Alvarez, P. Maximising the Deposition Rate of 5356 Aluminium Alloy by CMT-Twin-Based WAAM While Reducing Segregation-Related Problems by Local IR Thermography. *Metals* **2023**, *13*, 1890. https://doi.org/10.3390/met13111890

Academic Editors: Aleksander Lisiecki and Marcello Cabibbo

Received: 28 September 2023
Revised: 7 November 2023
Accepted: 10 November 2023
Published: 14 November 2023

Copyright: © 2023 by the authors. Licensee MDPI, Basel, Switzerland. This article is an open access article distributed under the terms and conditions of the Creative Commons Attribution (CC BY) license (https://creativecommons.org/licenses/by/4.0/).

1. Introduction

Wire and Arc Additive Manufacturing (WAAM) is growing in interest in different sectors such as aerospatial, maritime, and automotive, among others, and is being applied to many materials like aluminium alloys [1–3], steels [4], and titanium alloys [5]. Moreover, apart from materials, technologies used are going forward in order to obtain the best advantages of WAAM: high deposition rate, short time to market, and low Buy to Fly (BTF) ratio, making it suitable for the manufacturing of large parts. WAAM is characterised by the deposition of overlapped layers obtaining a near-net-shape part and it emerges as a practical solution for the manufacturing of high-dimension parts due to its high productivity potential and associated low manufacturing times and costs.

In order to optimise the BTF ratio, a tight selection of parameters needs to be used to minimise the surface waving and to avoid internal defects [1]. For that, a value of effective area gives a full vision of the percentage of the wall free of waving [6] and external defects.

Most associated defects in aluminium parts manufactured by WAAM are the porosity and solidification cracks [2,7,8]. Porosity is directly linked to the impairment of mechanical properties such as strength and ductility. This porosity normally appears due to the process parameters, heat input, alloy composition, interpass temperatures, and resulting microstructures [7].

CMT (Cold Metal Transfer) technology has been widely applied for the WAAM purposes of aluminium alloys, due to the lower heat input compared to other gas metal arc welding (GMAW) processes. The metal transference during CMT is assisted by the novel mechanical oscillation movement of the wire at high frequency [9]. Its coaxiality makes the deposition by WAAM easier regarding automation, path planning, and system complexity in comparison with other arc welding technologies such as gas tungsten arc welding (GTAW) and plasma arc welding (PAW) that need lateral wire feeding. A recent study [8] applied CMT to 5356 aluminium alloy and concluded that deposition strategy, shielding gas, and gas flow rate directly affect porosity.

In order to increase WAAM process efficiency, which is critical for the manufacturing of large components, different alternatives have been studied so far, including the increase in the welding current employed in conventional GMAW processes [10] and the deployment of multiple wire processes, such as tandem GMAW [11–13] and double-wire GTAW [14].

The tandem GMAW arc welding process is characterised by the combination of two independent welding sources that are fully synchronised [15,16]. Two filler metals are fed into a single torch hose pack via separate feeders and routed through electrically isolated contact tips [17]. A single shielding gas nozzle is employed and the two arcs generate a single weld pool. The possibility of isolating each power source and synchronising them allows for implementing CMT, pulsed, and other innovative welding curves independently, leveraging a range of process combinations. In this sense, the ancient double-wire welding GMAW technologies were limited by the fact that the electrodes were not isolated and the same potential should be selected for only standard GMAW welding curves. Being a tandem GMAW arc process, the state of the art CMT-Twin process provides the typical assisted droplet detachment of the CMT process which leads to low spatter and heat input, while either welding speed or deposition rate can be doubled [18]. Recently, these authors have investigated this innovative welding process for the WAAM of aluminium alloys [15,19–22].

Both tandem GMAW and CMT-Twin have been successfully employed to create in situ personalised alloys by combining different wires [18,21,23]. It also offers the possibility of increasing the deposition rates. This goal was studied in stainless steel by Martina et al. [24], with CMT doubling the deposition rate for thin parts; however, for the manufacturing of thicker parts without defects, an additional cooling aid was required.

In the case of the CMT unitary torch for 5356 alloy, Köhler et al. described a methodology to obtain sound walls that met the standards related to tensile properties for the wrought material [25]. In this case, the deposition rates achieved are between 1 and 1.2 kg/h. In order to manufacture big parts by WAAM, CMT-Twin allows for higher deposition rates, but the presence of two electric arcs increases the heat input. In this regard, heat input, heat distribution, and heat accumulation directly affect the geometry of the deposited part [25]. Due to this, a balance between deposition rate and surface waving needs to be found. According to Tawfik et al. [1,26], the obtained volume fraction of pores in 5356 aluminium alloy is directly proportional to heat input. Cracking is also due to the reheating caused by the successive deposition of layers, and it affects the mechanical properties.

Obtained dimensions, microstructures, and mechanical properties highly depend on the cooling conditions during the manufacturing of a part by WAAM [27,28]. The successive deposition of layers of the process itself affects the previously deposited layer, creating complex microstructures, but also being a source of possible defects such as pores and segregations [29]. With the aim of obtaining a homogenous microstructure and mechanical properties in the whole part, active cooling has been studied in recent works [25].

The use of forced cooling such as a cooling plate has been widely applied to avoid heat accumulation [28,30]. Moreover, the control of interpass temperature can be used as a strategy to prevent defects such as pores and cracks. Derekar et al. [2] concluded that an interpass temperature of 100 °C including a preheating of the substrate at the same

temperature before the deposition of the first layer for 5356 and an oscillating strategy reduced the amount and size of pores.

In the fusion line, other defects such as segregations (Al_8Mg_5) at the grain boundaries are also visible in WAAM manufactured parts of 5356 due to a long heat exposure at those zones [25]. These segregations and other heterogeneities in grain size and hardness affect the obtained mechanical properties in a vertical orientation, being poorer than in the horizontal orientation [25].

In order to monitor the temperature of the wall for a near-net-shape part by WAAM, other works used thermography as a monitoring technique to maintain a constant interpass temperature, avoiding the use of a constant interpass dwell time [31]. They observed that a constant interpass dwell time affects the final geometry, causing irregularities in the part weight and height.

The objective of this study was to find the highest deposition rate to manufacture a sound wall using CMT TWIN with 5356 aluminium alloy. Moreover, the effect of cooling conditions was studied by changing the interpass dwell time with the aid of thermography to monitor local temperature in the last deposited layer and the use of active cooling through a cooling plate in order to find an optimised deposition strategy with the lowest manufacturing time. Mechanical properties and microstructure are assessed to verify the best conditions.

2. Materials and Methods

WAAM parts were manufactured in an arc welding robotic cell. A Fronius TransPlus synergic (TPS) 4000 CMT R and 5000 CMT R power sources, two fully digital inverter CMT welding power sources, and a Robacta Twin Compact Pro 30° PA OVT torch from Fronius International (Fronius International, Wels, Austria) were used. A scheme of the torch and the created electric arc is shown in Figure 1.

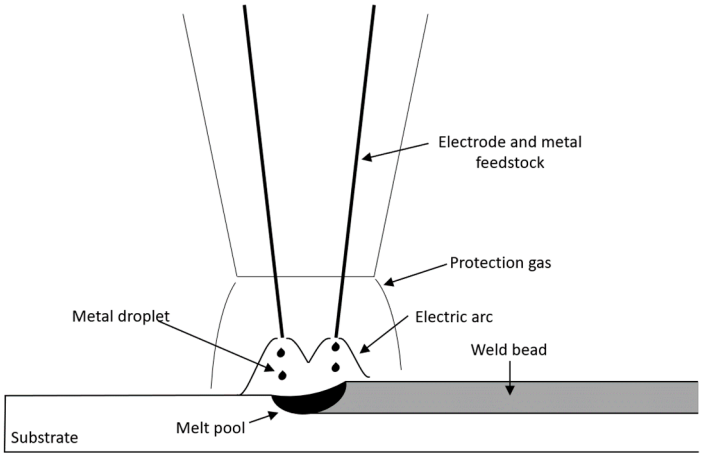


Figure 1. Scheme of CMT TWIN two electric arcs.

The welding torch was attached to a 6-axis ABB robot IRB 4600-45/2.05 model with a IRC5 controller (ABB Ltd., Zurich, Switzerland. The gas shielding of the torch was carried out with Argon (99.999% purity) and the gas flow was set at 25 L/min. A 1.2-mm diameter ER5356 wire from ESAB was employed as filler metal. The substrates for the manufacturing of the walls were of AA6082-T6 alloy. The chemical compositions of the wire and the substrate are shown in Table 1.

Table 1. Chemical composition of the wire and the substrate in wt. %.

Alloy	Chemical Composition (wt. %)							
	Al	**Cr**	**Cu**	**Fe**	**Mg**	**Mn**	**Si**	**Ti**
AA5356 (ER5356)	Bal.	0.05–0.20	≤0.10	≤0.40	4.5–5.5	0.05–0.20	≤0.25	0.06–0.20
Al6082-T6	Bal.	≤0.25	≤0.10	≤0.50	0.60–1.20	0.40–1.0	0.70–1.30	≤0.10

In order to check the temperature during the deposition and heat accumulation, K-type thermocouples were welded to the substrate. Their location is shown in Figure 2 with 2 stars named T1 related to thermocouple 1 and T2 related to thermocouple 2. The distance between the walls and the thermocouples is 50 mm.

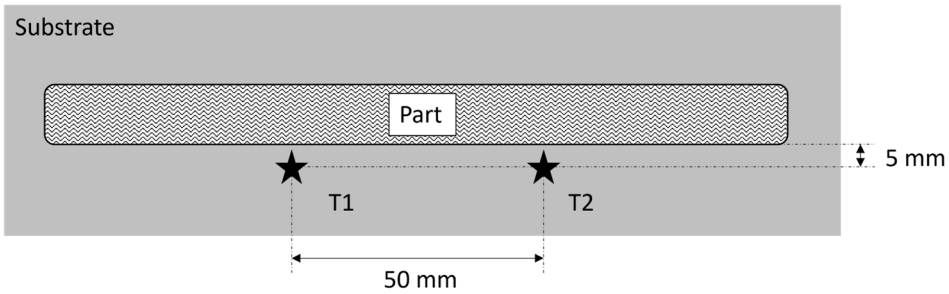


Figure 2. Scheme of the thermocouples attached to the substrate.

The setup for the manufacturing of the walls is shown in Figure 3. It includes a cooling plate with internal water conformal cooling connected to a chilling machine. The substrate was clamped to this cooling plate to achieve forced cooling conditions.

For the local thermal analysis, a Flir a655sc microbolometer infrared camera (Teledyne FLIR LLC, Wilsonville, OR, USA) was employed. The spectral range of the camera is 7–14 µm and its temperature calibration is up to 2000 °C. Standard 25.4 mm lenses were employed and the whole system was encapsulated. The frame rate employed was 16 frames/s. The camera was mounted on a tripod and placed at one side of the component at an approximate distance of 40 cm from the deposition zone. The temperature was always captured at the last deposited layer. The measurement of the temperature was obtained after 30 s once the torch passed.

For the first assessment of welding parameters to optimise the deposition rate, walls of 10 layers were built. In a second assessment, taller walls were manufactured (70 × 130 mm^2) to check the influence of heat accumulation and mechanical properties in horizontal and vertical orientations. Pulse mode was used for the leading wire, whereas CMT mode was applied to the trailing wire.

Two different deposition strategies were used: circling and hatching. Circling strategy means an overlapping of round circles with 2 mm of amplitude and 3 Hz frequency. Ignition and extinction of the electric arc was alternated between layers in order to avoid material accumulation. A scheme of both strategies is shown in Figure 4.

The orientation of the torch is perpendicular to the substrate. The offset in Z direction was continuously adjusted in a range of 2–2.5 mm in order to maintain a constant voltage. Depending on the interpass dwell time used and the height of the wall, the Z offset value needs to be adjusted. This interpass dwell time is defined as the time in which the arc is stopped between the deposition of consecutive layers.. The study of interpass dwell times (30, 60, 90, 120, 180, and 240 s) and the use of a cooling plate (with and without) was conducted as shown in Table 2 where X means that the experiment was conducted and - no.

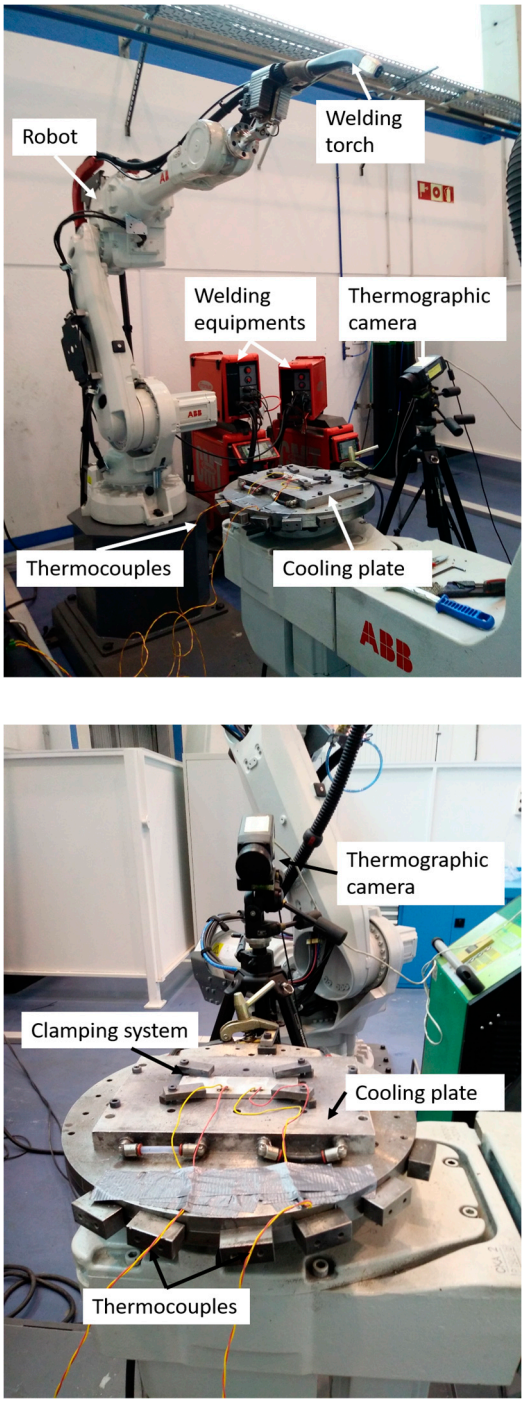


Figure 3. Setup for the manufacturing of the walls.

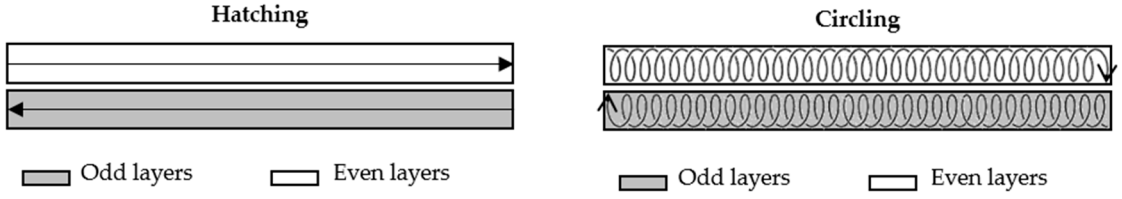


Figure 4. Scheme of hatching and circling strategies composed by repeated pair of layers.

Table 2. Experiments performed with different interpass dwell times and the use of a cooling plate.

	Interpass Dwell Time (s)					
Cooling Plate	**30**	**60**	**90**	**120**	**180**	**240**
With	X	X	X	X	X	X
Without	X	X	X	X	-	-

Samples were cut for microstructural characterisation and measurement of the effective area in the cross section. After cutting the samples, they were mounted, polished, and etched. Light microscopy images were taken with an Olympus GX51 microscope (Olympus Corp., Tokyo, Japan). Internal defects such us porosity and segregations were also evaluated by measurement along the height of the wall. Edges of walls were discarded for this analysis.

Mechanical characterisation was carried out in X direction (horizontal) and Z direction (vertical). The flat dog-bone tensile test specimens were extracted from the walls, according to the ASTM E8M standard [32], by using an electron discharge machine as shown in Figure 5. Six samples were tested for each set of cooling conditions. Tensile tests were performed in a Z100 ZWICK/Roell testing machine (ZwickRoell S.L., Barcelona, Spain) with a maximum load capacity of 100 kN. Specimens were tested at room temperature with a displacement rate of 1.6 mm/min and an extensometer with a gauge length of 25 mm.

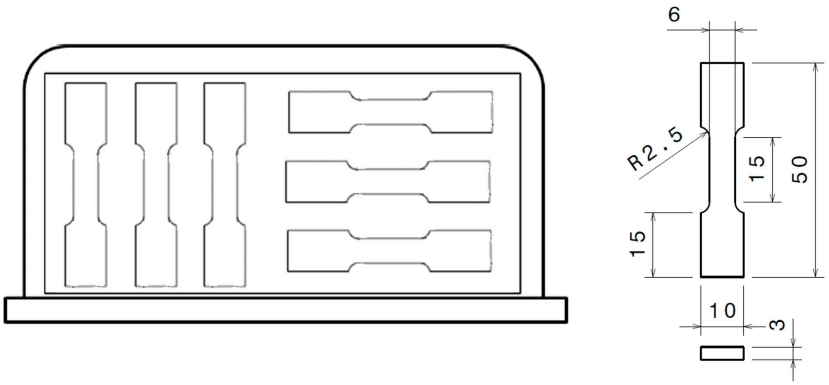


Figure 5. Scheme of the location of tensile samples and their dimensions in mm.

3. Results

3.1. Manufacturing Process Optimisation

The preliminary parameters studied for each deposition strategy and their corresponding heat input and deposition rates are shown in the Table 3. Bead-on-plate weld beads were used to find the best conditions for WAAM manufacturing.

Table 3. Tested welding parameters and strategies.

Set of Parameters	WS (m/min)	Deposition Strategy	WFS (m/min) Lead	WFS (m/min) Trail	Current (A) Lead	Current (A) Trail	Voltage (V) Lead	Voltage (V) Trail	Heat Input (KJ/cm)	Deposition Rate (kg/h)
1	0.6	Hatching	5	5	79	91	14.8	10.2	1.68	1.79
2	0.6	Hatching	8	8	121	119	15.8	11	2.58	2.87
3	0.6	Hatching	10	10	150	145	16.2	11.8	3.31	3.58
4	0.6	Circling	5	5	79	91	14.8	12.6	1.85	1.79
5	0.6	Circling	8	8	121	119	15.8	13.4	2.81	2.87
6	0.6	Circling	10	10	150	145	16.2	14.2	3.59	3.58

In Figure 6, the cross section of the weld beads of each set of parameters can be observed. The measured geometry of them can be shown in Table 4. Hatching strategy (set

of parameters 1, 2, 3) did not obtain full wetting between the weld bead and the substrate (indicated with white arrows).

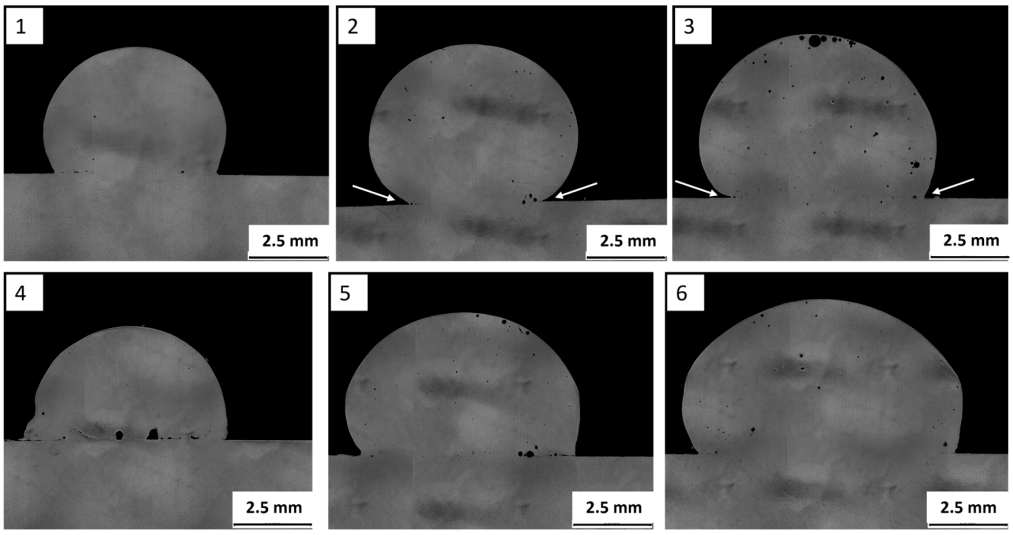


Figure 6. Weld bead cross section for different set of parameters (1 to 6) shown in Table 3. White arrows indicate insufficient wetting.

Table 4. Geometry of the weld bead sections for each set of parameters.

Set of Parameters	Width (mm)	Height (mm)
1	6.1	4.3
2	7.0	5.3
3	7.9	5.5
4	6.8	3.8
5	7.8	4.8
6	9.4	5.1

Circling strategy (length 3, width 2) obtained better wetting angles with the substrate; however, the highest deposition rate (set of parameters 6) was discarded due to an excessive thickness of the weld bead which did not meet the required geometry for the homogeneous growth of a part by the successive deposition of weld beads.

Finally, the conditions of set of parameters 5 were selected to manufacture sound parts with a wall shaped to study the influence of the cooling conditions.

3.2. Forced Cooling

The wall manufactured using 30 s of interpass dwell time with a cooling plate is shown in Figure 7. It shows a regular growth, considered appropriate for part manufacturing.



Figure 7. (**a**) Wall manufactured with 30 s of interpass dwell time using the cooling plate and (**b**) cross section.

The temperature profiles for the interpass dwell time of 30 s with and without the cooling plate recorded by the thermocouples attached to the substrate are shown in Figure 8. This interpass dwell time infers the highest temperature to the manufactured wall. Clearly, the use of the cooling plate helps avoid heat accumulation from the first deposited layer with a difference in constant temperature of around 75 °C.

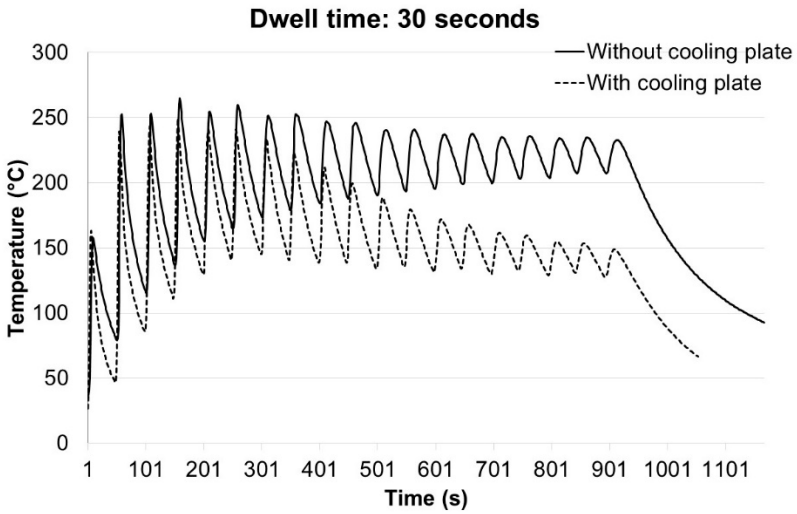


Figure 8. Temperature evolution graph measured for 30 s of interpass dwell time comparing the use of the cooling plate.

In Figure 9, the average of the plateau zone of the interpass temperature measured from the temperature records of each studied condition has been collected.

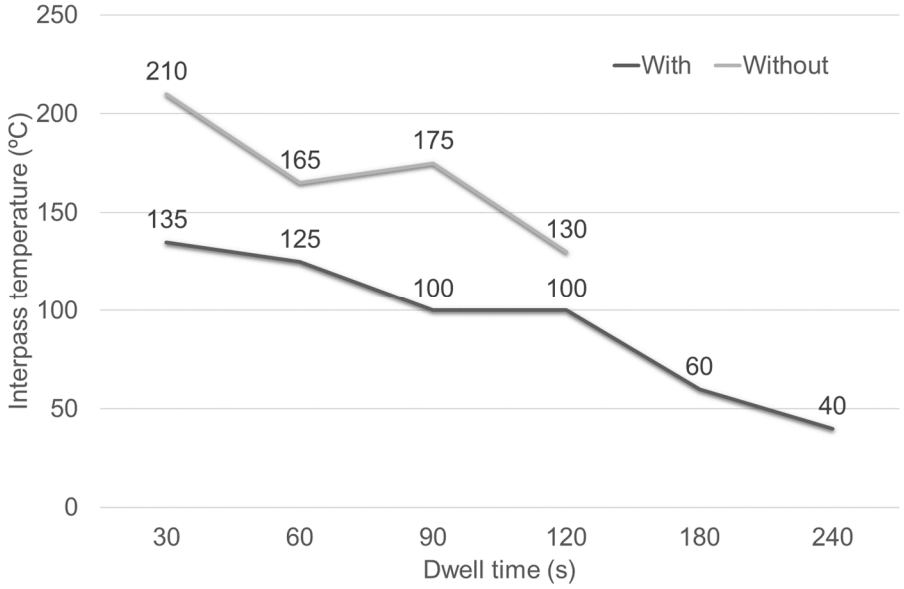


Figure 9. Values of the constant interpass temperature for each condition.

Increasing the interpass dwell time helps to reduce interpass temperature between layer deposition. The use of the cooling plate also reduces the interpass temperature.

The dimensions of the manufactured walls for each cooling condition, maintaining the same manufacturing parameters, were measured. They are shown in Figure 10. In this graph, it can be observed that the thickest walls are obtained for the lowest dwell time and the thinnest ones for the highest dwell time. In contrast, regarding the height, the shortest wall is the one with the lowest dwell time and the tallest wall is the one with the highest

dwell time. The influence of the use of the cooling plate is seen by decreasing the width and increasing the height.

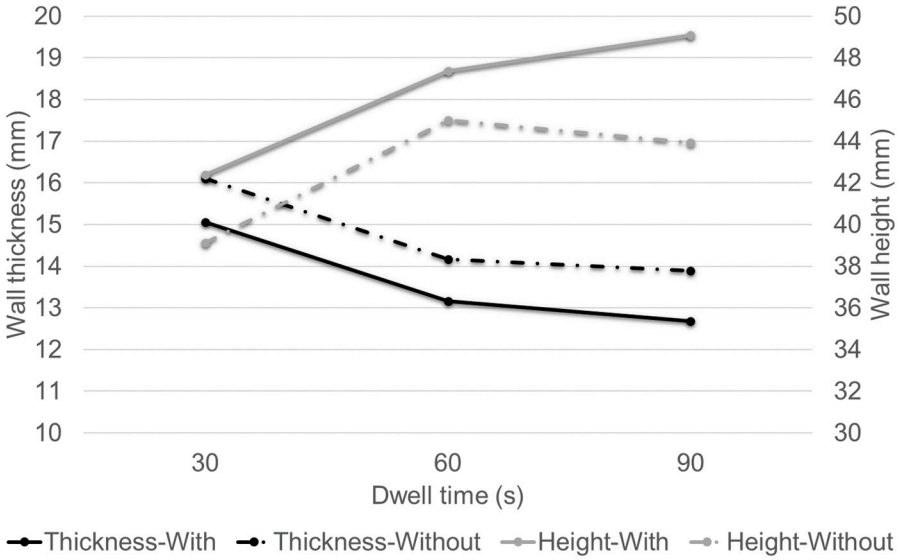


Figure 10. Thickness and height of walls for different cooling conditions: with and without the cooling plate.

3.3. Microstructural Analysis

In the first attempt with the selected parameters and interpass dwell times (30, 60, and 90 s), all the manufactured walls presented segregations and pores (Figure 11a) in their cross sections, which appeared from a specific layer height up to the top of the wall. These segregations were located between the deposited layers as shown in Figure 11b. They appeared from the external faces of the wall, and they reached deeper in the wall as the height of the wall increased.

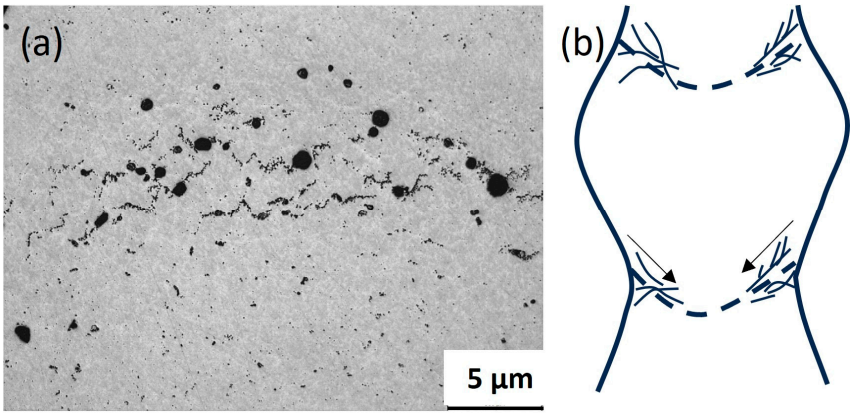


Figure 11. (**a**) Segregations detected in the cross section of the wall manufactured using an interpass dwell time of 60 s. (**b**) Scheme with the location of the segregations.

In Table 5, the effective area showed a clear decrease when reducing interpass dwell time. The effective area is the largest rectangle that can be shaped in the cross section. In this case, it is not just affected by the waving of the surface but also by the segregations. Figure 12 shows the total area, effective area without waving and effective area without segregations obtained from a cross section of a wall. The decreasing trend observed is the same considering the removal of waving and the removal of segregations to obtain the sound part.

Table 5. Calculated effective area for different interpass dwell times using a cooling plate.

Interpass Dwell Time (s)	Effective Area (%)	Effective Area (%)
	Without Waving	Without Segregations
90	88	76
60	83	86
30	85	63

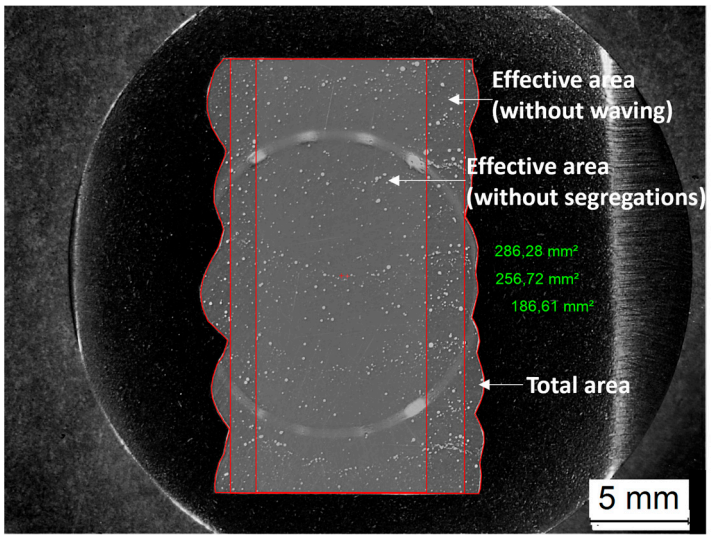


Figure 12. Cross section of a WAAM wall where total area, effective area without waving and effective area without segregations are indicated.

The height at which the segregations appeared for each used interpass dwell time is shown in Figure 13. Clearly, the height at which the first segregation appears is higher for longer interpass dwell times. When no cooling plate is used (120 N), the first segregations appear at a lower height.

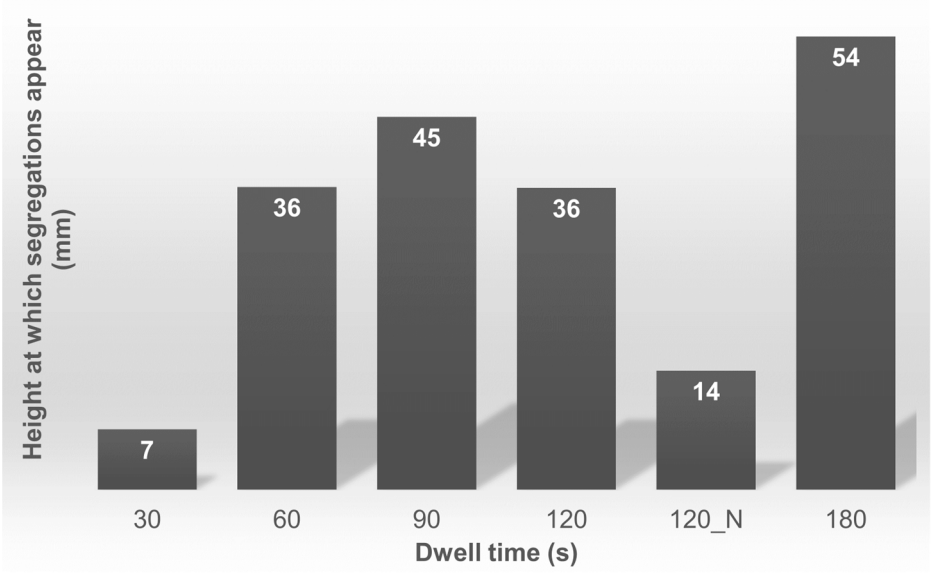


Figure 13. Height at which segregations appear in walls manufactured with different interpass dwell times using a cooling plate except where stated "N", meaning no cooling plate was used.

3.4. Interpass Dwell Time Optimisation

To avoid these segregations, thermography was used to measure the temperatures at the melt pool and find the limit temperature that induces segregations when exceeded. Boxes were located in the centre line of the base (Box 1), centre (Box 2), and top (Box 3) of the wall to obtain the temperature measurements (Figure 14). The thermal signal below the torch was saturated as the maximum temperature of the camera (600 °C) was exceeded. When the signal obtained in the box was not saturated, the acquisition of frames for the analysis started.

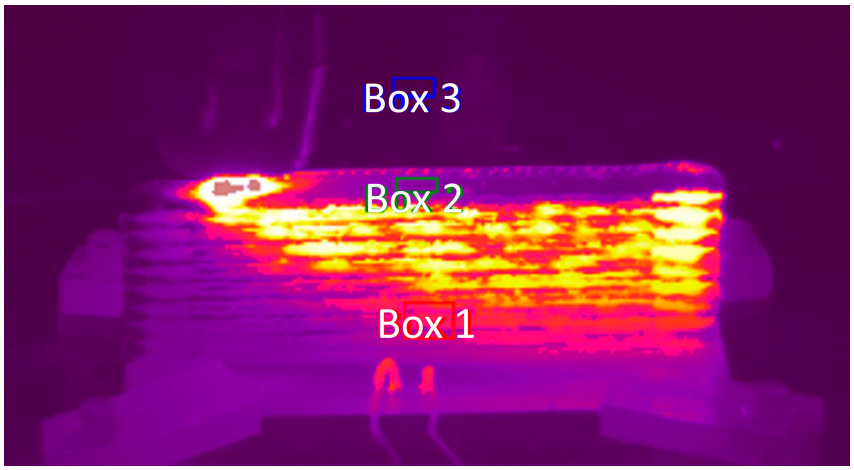


Figure 14. Thermographic image of the wall and location of the boxes for the temperature measurement.

The graph shown in Figure 15 represents the main temperature values obtained during 200 frames (equivalent to 30 s) after the maximum temperature detected in the three located boxes for the wall manufactured with 120 s of interpass dwell time without a cooling plate.

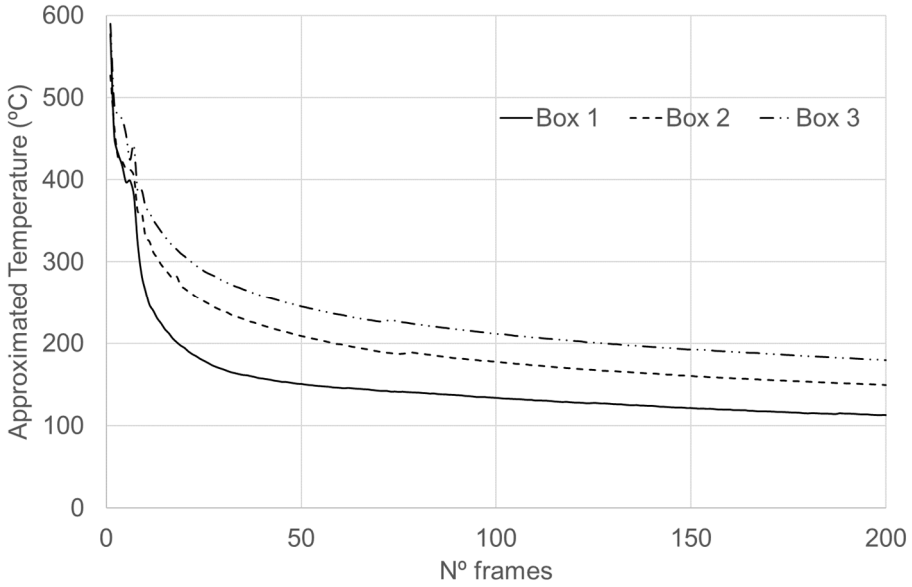


Figure 15. Main temperature evolution in the 3 boxes of the wall with 120 s of interpass dwell time without cooling plate.

In the Table 6, the main temperatures measured in the base, centre, and top of the wall for the different conditions of interpass dwell time and use of the cooling plate at frame 200 can be observed. Shadowed cells correspond to the zones where segregations were found. The height of the boxes was related to the location of segregations detected

through metallography in the walls. The lowest temperature detected at which segregations appeared was 146 °C.

Table 6. Temperature measured in the 3 boxes of the walls and the presence of segregations for each condition (shadowed cells).

		Wall Zone			
Interpass Dwell Time (s)	**Cooling Plate**	**Base**	**Centre**	**Top**	**Segregations**
120	WITHOUT	112	149	179	YES
120	WITH	150	163	173	YES
180	WITH	116	126	146	YES
240	WITH	127	124	128	NO

Therefore, an optimised wall with varying interpass dwell time was proposed to reduce the manufacturing time ensuring a sound part considering the height where segregations appeared and measuring temperature. The limit temperature to define the optimised interpass dwell time was established at 140 °C. The stated interpass dwell time for each range of layers for the optimised wall is defined in Table 7.

Table 7. Defined interpass dwell time to obtain a sound wall with optimised manufacturing time.

Layers		
From	**To**	**Interpass Dwell Time (s)**
0	1	30
1	9	60
9	14	90
14	18	120
18	21	180
21	35	240

As expected, no segregations appeared in the optimised wall.

3.5. Mechanical Properties

The mechanical properties obtained for the different interpass dwell times for both orientations can be observed in Table 8. The mechanical properties obtained from the walls fabricated with CMT-Twin were manufactured using the cooling plate. To be compared, the mechanical properties obtained from the walls manufactured by unitary torch CMT and without the cooling plate from the work of Arana et al. [8] have been included in the same table. It can be observed that the values are similar between the different interpass dwell times used.

Anisotropy is detected, obtaining both lower elongation and strength in the vertical orientation. As seen in Table 9, the lowest anisotropy in elongation (5%) is detected for the longest interpass dwell time (240 s) while the largest one (27%) is obtained with the lowest interpass temperature (90 s). The anisotropy in strength is always below 4%, obtaining the lowest anisotropy for the longest interpass dwell time (240 s).

Table 8. Tensile properties obtained for different interpass dwell times and orientations with CMT-Twin.

Interpass Dwell Time (s)	Orientation	$Rp_{0.2}$ (MPa)	R_m (MPa)	e (%)
90	Vertical	106.9 ± 3.4	244.9 ± 9.1	19.8 ± 4.4
90	Horizontal	115.7 ± 12.1	264.4 ± 9.2	34.4 ± 0.8
90 (unitary torch without cooling plate)	Vertical	113 ± 0.9	277 ± 2.1	29.2 ± 2.7
90 (unitary torch without cooling plate)	Horizontal	124 ± 11.9	277 ± 1.2	29.9 ± 0.7
120	Vertical	107.6 ± 3.3	256.9 ± 3.7	25.9 ± 2.0
120	Horizontal	111.8 ± 7.9	263.0 ± 7.5	35.0 ± 0.6
180	Vertical	104.6 ± 2.9	256.9 ± 3.7	29.8 ± 0.7
180	Horizontal	114.1 ± 1.8	264.1 ± 5.5	30.7 ± 1.4
240	Vertical	109.7 ± 4.5	259.2 ± 3.5	29.4 ± 1.23
240	Horizontal	108.2 ± 3.5	259.1 ± 2.3	32.7 ± 0.6
OPT	Vertical	113.5 ± 2.1	258.5 ± 3.2	23.6 ± 2.9
OPT	Horizontal	115.4 ± 0.7	266.7 ± 1.5	33.7 ± 0.8

Table 9. Calculated anisotropy of the obtained mechanical properties.

			Anisotropy		
Torch	**Dwell Time (s)**	**Cooling Plate**	**YS (Mpa)**	**UTS (Mpa)**	**e (%)**
TWIN	90	With	4%	4%	27%
Unitary	90	Without	4%	0%	1%
TWIN	120	With	2%	1%	15%
TWIN	180	With	4%	1%	1%
TWIN	240	With	1%	0%	5%
TWIN	OPT	With	1%	2%	18%

4. Discussion

The selected weld bead for the growth of the walls assures a minimum and stable surface waving. Heat input was said to greatly influence increasing the width of the weld bead, whereas the height decreased in a lower way [30]. Moreover, the circling strategy gave rise to thicker weld beads and hence a more stable and homogenous growth of the wall. This was also observed in previous works with the unitary torch [8]. Concretely, in this case, the comparable dimensions of the weld bead were 8.0 mm of thickness and 3.7 mm of height.

Regarding manufactured walls with the different cooling conditions, shown in Figure 10, the one using the lowest interpass dwell time (30 s) without the use of a cooling plate had the lowest height (39.1 mm) and the largest width (16.1 mm). On the contrary, the one using the largest interpass dwell time (90 s) with the use of a cooling plate had the largest height (49.1 mm) and the lowest width (12.7 mm). These results were expected following the same trend as the dimensions of the weld beads (Table 4).

Cracking has been found due to the heat accumulation which forms low melting point segregations during the cooling stage as shown in Figure 16. Therefore, we can observe them in a high amount once the wall grows in height because the heat dissipation becomes more difficult and then the interpass temperature increases, so the cooling rate greatly decreases.

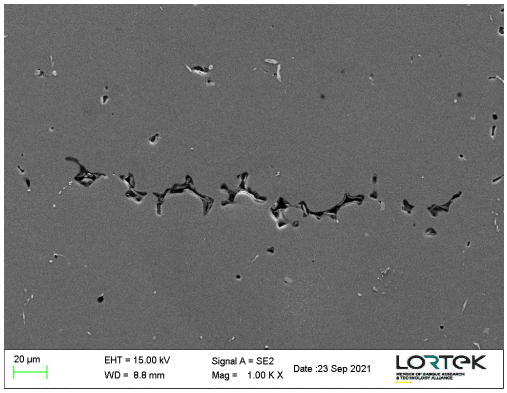


Figure 16. Merged segregations formed.

An interlayer boundary zone with a further increased occurrence of segregations can be identified (Figure 11b). In these regions, primary stages and segregations merged at the grain boundaries as a result of comparatively long heat exposure giving rise occasionally to cracks. Even if the cracks are not opened, due to the difference in hardness, grain size, and the formation of segregations, these areas can act as metallurgical notches, thus affecting the mechanical properties in the vertical loading direction, as can be observed in Table 8.

As stated in other works, the increase in deposition rate requires additional cooling as found with other materials such as steel [24]. As observed in Figure 9, the effect of the use of the cooling plate in the interpass temperature can be clearly seen; however, it is more noticeable for shorter interpass dwell times, when the substrate is at higher temperatures. Other kinds of forced cooling [33] could be of help in decreasing the interpass temperature in a greater amount; however, the obtained microstructure can be affected by obtaining supersaturated solid solution hard phases [27] and affecting the mechanical properties.

Segregations are detected higher in the wall for an interpass dwell time of 120 s without using the cooling plate. In this case, the height at which the first segregations appear (14 mm) is close to the one measured for an interpass dwell time of 30 s (7 mm) using the cooling plate. This implies a reduction in time of fabrication.

The interpass temperature measured with the unitary torch using 90 s of interpass dwell time between layer deposition is 85 °C [8] and 175 °C in the same conditions with TWIN torch. Comparing the heat input for the used welding parameters with TWIN torch it is 2.81 KJ/cm versus 0.72 KJ/cm for the unitary torch. Nevertheless, the use of TWIN presents interesting advantages compared with the unitary torch such as the higher deposition rate (2.87 kg/h vs. 0.93 kg/h [8]) for the same material and without considering the interpass dwell time. Moreover, as shown in Table 10, with the optimisation of interpass dwell time, the sum of the interpass dwell time needed for the deposition of 20 layers was equal with both torches: 30 min. The higher deposition rate obtained by the TWIN torch comprehends both of the following: higher layer height (2.36 vs. 1.85 mm) and higher layer width (12 vs. 6.2 mm) for the same welding speed.

Table 10. Comparison between the walls manufactured with unitary and with TWIN torches for 5356.

Torch	Forced Cooling	Deposition Rate (kg/h)	HI (KJ/cm)	Total Interpass Dwell Time for 20 Layers (s)	Width (mm)	Height per Layer (mm)	Ws (m/min)
Unitary [8]	NO	0.93	0.72	1800	6.2	1.85	0.6
TWIN	YES	2.87	2.81	1800	12	2.36	0.6

The use of the interpass dwell time of 240 s makes the advantages of TWIN disappear. This interpass dwell time has been optimised by adjusting it to the temperature of the wall, since closer layers to the substrate can dissipate the heat more easily than the more distant ones and hence the heat accumulates with a growth in height [13,34]. In Table 11 the total

interpass dwell time used, and the presence of segregations, can be seen for 35 layered walls. The difference between the optimised wall and the wall with 240 s of interpass dwell time is close to 1 h. This manufacturing time is around 150 s of constant interpass dwell time, this being an acceptable interpass dwell time for an industrial approach. Real parts usually require manufacturing times of each individual layer equivalent or higher than the interpass dwell times. Moreover, a proper interpass dwell time helps increase the effective area as seen in Table 5 [27] and the height and thickness per layer grown also increases as shown in Table 10. This optimisation of interpass dwell time gave rise to a reduction in manufacturing time of 36%.

Table 11. Relation between total interpass dwell time for 35 layered walls, presence of segregations, and interpass dwell time.

Interpass Dwell Time	Total Interpass Dwell Time	Presence of Segregations
30 s	17.5 min	YES
60 s	35 min	YES
90 s	52.5 min	YES
120 s	1 h 10 min	YES
Optimised	1 h 29 min	NO
180 s	1 h 45 min	YES
240 s	2 h 20 min	NO

Thermography was demonstrated to be a useful tool to locate the temperature and segregations to define the limit temperature to avoid segregations. Optimising the setup would help to improve the quality of the obtained results. To do so, the camera should be placed on a zenithal position with respect to the weld. By doing this, the effect of the emissivity could be homogenised. Together with this, a wider range of temperatures should be employed, in order to avoid saturation on the torch. Regarding the extracted data, further analysis should be performed, focusing not only on the final temperature after 30 s, but also on the cooling rate of the curves, which could offer more accurate information about the crack generation.

Regarding the mechanical properties, optimal results were obtained even for the shorter interpass dwell times where segregations could be found in the wall cross section. However, as stated before, these segregations appear from the surface of the wall, whereas the tensile samples were extracted from the medium zone of the wall, and therefore the cracks did not reach the tensile samples. However, in a real part, those defects must be avoided, because the BTF ratio increases as the effective area decreases (Table 5). Obtained tensile values are similar to the ones revealed for WAAM in other works [8,29,35] and higher compared to the main providers' material specifications. Moreover, taking into account the average of the obtained mechanical properties (Table 12) for the different interpass dwell times, they reveal deviations of less than 3 Mpa, which means that the used interpass dwell times do not induce substantial differences in the microstructure apart from the appearance of segregations in the outer zones. In the work from Derekar et al. [2], for the same material, a slight difference in mechanical properties was observed (4 Mpa) when comparing two interpass temperatures (50 °C and 100 °C), obtaining better properties for 100 °C of interpass temperature due to the larger grain size, and the lower amount and smaller pores. In this work, the interpass temperature is above 100 °C in all the cases, which can induce large grain size and the typical inhomogeneous microstructure due to the continuous thermal cycles of the process, and hence the mechanical properties are not significantly affected by the changes in the interpass dwell time. This was also observed in the work of Köhler et al. [25].

Table 12. Average mechanical properties for the different interpass dwell times.

YS (Mpa)	UTS (Mpa)	e (%)
110.8 ± 2.3	259.4 ± 2.9	29.5 ± 1.6

Anisotropy in elongation is more evident at low interpass dwell times (27% for 90 s of interpass dwell time vs. 5% for 240 s of interpass dwell time) where horizontal orientation obtained higher results in terms of strength and elongation as found in other works [25,29,35] and compared to the unitary torch [8]. This is principally explained by the heterogeneity and defects between layers [25]. The lower anisotropy has been obtained for the longest interpass dwell time (240 s), and for the unitary torch without a cooling plate (90 s). This suggests the importance of maintaining a low interpass temperature. In the case of manufacturing with CMT-Twin, it has been observed that there is a need for a cooling plate in addition to longer interpass dwell times to maintain a low interpass temperature. The optimised wall obtained 18% of anisotropy in elongation. This might be improved if a constant interpass temperature is maintained during the wall manufacturing.

5. Conclusions

CMT-Twin technology was demonstrated to be an interesting option for obtaining sound walls by WAAM with high effective area and high deposition rate oriented to parts with a minimum thickness of 10 mm. In these terms, the deposition rate compared to a unitary torch is three times higher.

The use of the CMT-Twin torch increases the deposition rate compared to the unitary torch; however, the heat input increases as well. A proper manufacturing strategy must be defined to avoid cracking, in order to obtain optimal mechanical properties. The use of thermography allowed us to determine the temperature during the process and to define a limit temperature to avoid segregations and cracking.

The use of a cooling plate demonstrated that it reduces the heat accumulation in a high amount. Its effect is more obvious for short interpass dwell times. It was also determined that the use of CMT-Twin requires extra cooling conditions (longer interpass dwell time and a cooling plate) to obtain sound parts.

An optimised interpass dwell time applied per range of layers combined with forced cooling reduces total interpass dwell time by around 1 h assuring no segregations. This, together with the three times higher deposition rate, makes this method of high interest.

The mechanical properties obtained revealed anisotropy mostly for lower interpass dwell times, with the horizontal orientation being the one obtaining higher results both in strength and elongation. Values for the longest interpass dwell time (240 s) and the use of a cooling plate are comparable to the values obtained in other works where interpass dwell time was 90 s without the use of a cooling plate.

Author Contributions: Conceptualization, L.V. and P.A.; methodology, A.I., P.L.d.U. and L.V.; validation, P.A.; formal analysis, L.V.; investigation, L.V., A.I. and P.L.d.U.; resources, P.A.; data curation, L.V. and P.L.d.U.; writing—original draft preparation, L.V.; writing—review and editing, L.V. and P.A.; supervision, P.A.; funding acquisition, P.A. All authors have read and agreed to the published version of the manuscript.

Funding: This project has received funding from the European Union's Horizon 2020 research and innovation programme under grant agreement No. 862617 MULTI-FUN project: Enabling MULTI-FUNctional performance through multi-material additive manufacturing.

Data Availability Statement: Data available on request due to restrictions. The data presented in this study are available from the corresponding author.

Conflicts of Interest: The authors declare no conflict of interest.

References

1. Tawfik, M.M.; Nemat-Alla, M.M.; Dewidar, M.M. Effect of Travel Speed on the Properties of Al-Mg Aluminum Alloy Fabricated by Wire Arc Additive Manufacturing. *J. Mater. Eng. Perform.* **2021**, *30*, 7762–7769. [CrossRef]
2. Derekar, K.; Lawrence, J.; Melton, G.; Addison, A.; Zhang, X.; Xu, L. Influence of Interpass Temperature on Wire Arc Additive Manufacturing (WAAM) of Aluminium Alloy Components. *MATEC Web Conf.* **2019**, *269*, 05001. [CrossRef]
3. Li, S.; Zhang, L.J.; Ning, J.; Wang, X.; Zhang, L.L.; Long, J.; Zhou, X.R.; Na, S.J. Microstructures and properties of wire-arc additively manufactured 5356 aluminium alloy protected by different proportions of nitrogen and argon. *J. Mater. Sci.* **2021**, *56*, 17785–17804. [CrossRef]
4. Rodriguez, N.; Vázquez, L.; Huarte, I.; Arruti, E.; Tabernero, I.; Alvarez, P. Wire and Arc Additive Manufacturing: A comparison between CMT and TopTIG processes applied to Stainless Steel. *Weld. World* **2018**, *62*, 1083–1096. [CrossRef]
5. Zhang, X. Structural Integrity Performance of Additively Manufactured Titanium Alloys. Royal Aeronautical Society Structures and Materials Conference, Sheffield. 2017. Available online: https://www.aerosociety.com/media/5410/4-durability-and-damage-tolerance-performance-of-additive-manufactured-ti-6al-4v-titanium-alloy.pdf (accessed on 9 November 2023).
6. Waqas, A.; Qin, X.; Xiong, J.; Wang, H.; Zheng, C. Optimization of process parameters to improve the effective area of deposition in GMAW-based additive manufacturing and its mechanical and microstructural analysis. *Metals* **2019**, *9*, 775. [CrossRef]
7. Gierth, M.; Henckell, P.; Ali, Y.; Scholl, J.; Bergmann, J.P. Wire Arc Additive Manufacturing (WAAM) of aluminum alloy AlMg5Mn with energy-reduced Gas Metal Arc Welding (GMAW). *Materials* **2020**, *13*, 2671. [CrossRef] [PubMed]
8. Arana, M.; Ukar, E.; Rodriguez, I.; Iturrioz, A.; Alvarez, P. Strategies to reduce porosity in Al-Mg WAAM parts and their impact on mechanical properties. *Metals* **2021**, *11*, 524. [CrossRef]
9. Chen, X.; Kong, F.; Fu, Y.; Zhao, X.; Li, R.; Wang, G.; Zhang, H. A review on wire-arc additive manufacturing: Typical defects, detection approaches, and multisensor data fusion-based model. *Int. J. Adv. Manuf. Technol.* **2021**, *117*, 707–727. [CrossRef]
10. Xiong, J.; Zhang, G.; Zhang, W. Forming appearance analysis in multi-layer single-pass GMAW-based additive manufacturing. *Int. J. Adv. Manuf. Technol.* **2015**, *80*, 1767–1776. [CrossRef]
11. Guangchao, L.; Xiong, Y.; Tang, L. Microstructure and mechanical properties of 2219 aluminum alloy fabricated by double-electrode gas metal arc additive manufacturing. *Addit. Manuf.* **2020**, *35*, 101375. [CrossRef]
12. Shi, J.; Li, F.; Chen, S.; Zhao, Y. T-GMAW based novel Multi-node trajectory planning for fabricating grid stiffened panels: An efficient production technology. *J. Clean. Prod.* **2019**, *238*, 117919. [CrossRef]
13. Shi, J.; Li, F.; Chen, S.; Zhao, Y.; Tian, H. Effect of in-process active cooling on forming quality and efficiency of tandem GMAW–based additive manufacturing. *Int. J. Adv. Manuf. Technol.* **2019**, *101*, 1349–1356. [CrossRef]
14. Ye, D.; Hua, X.; Wu, Y. Arc interference behavior during twin wire gas metal arc welding process. *Adv. Mater. Sci. Eng.* **2013**, *2013*, 937094. [CrossRef]
15. Yin, L.; Wang, J.; Hu, H.; Han, S.; Zhang, Y. Prediction of weld formation in 5083 aluminum alloy by twin-wire CMT welding based on deep learning. *Weld. World* **2019**, *63*, 947–955. [CrossRef]
16. Pickin, C.G.; Williams, S.; Prangnell, P.; Derry, C.; Lunt, M. Control of weld composition when arc welding high strength aluminium alloys using multiple filler wires. *Sci. Technol. Weld. Join.* **2010**, *15*, 491–496. [CrossRef]
17. Extended Information. Available online: www.fronius.com/en/welding-technology/product-information/tpsi-twin-systeme-tandem-welding (accessed on 9 November 2023).
18. Wang, Y.; Konovalov, S.; Chen, X.; Ivanov, Y.; Jayalakshmi, S.; Singh, R.A. Research on Cu-6.6%Al-3.2%Si Alloy by Dual Wire Arc Additive Manufacturing. *J. Mater. Eng. Perform.* **2021**, *30*, 1694–1702. [CrossRef]
19. Gu, J.; Bai, J.; Ding, J.; Williams, S.; Wang, L.; Liu, K. Design and cracking susceptibility of additively manufactured Al-Cu-Mg alloys with tandem wires and pulsed arc. *J. Mater. Process. Technol.* **2018**, *62*, 10. [CrossRef]
20. Pickin, C.G.; Williams, S.W.; Prangnell, P.B.; Robson, J.; Lunt, M. Control of weld composition when welding high strength aluminium alloy using the tandem process. *Sci. Technol. Weld. Join.* **2009**, *14*, 734–739. [CrossRef]
21. Klein, T.; Birgmann, A.; Schnall, M. In situ alloying of aluminium-based alloys by (multi-)wire-arc additive manufacturing. *MATEC Web Conf.* **2020**, *326*, 01003. [CrossRef]
22. Wang, S.; Gu, H.; Wang, W.; Li, C.; Ren, L.; Wang, Z.; Zhai, Y.; Ma, P. Study on microstructural and mechanical properties of an Al-Cu-Sn alloy wall deposited by double-wire arc additive manufacturing process. *Materials* **2020**, *13*, 73. [CrossRef]
23. Qi, Z.; Cong, B.; Qi, B.; Sun, H.; Zhao, G.; Ding, J. Microstructure and mechanical properties of double-wire + arc additively manufactured Al-Cu-Mg alloys. *J. Mater. Process. Technol.* **2018**, *255*, 347–353. [CrossRef]
24. Martina, F.; Ding, J.; Williams, S.; Caballero, A.; Pardal, G.; Quintino, L. Tandem metal inert gas process for high productivity WAAM in stainless steel. *Addit. Manuf.* **2019**, *25*, 545–550. [CrossRef]
25. Köhler, M.; Hensel, J.; Dilger, K. Effects of thermal cycling on wire and arc additive manufacturing of al-5356 components. *Metals* **2020**, *10*, 952. [CrossRef]
26. Tawfik, M.M.; Nemat-Alla, M.M.; Dewidar, M.M. Enhancing the properties of aluminum alloys fabricated using wire + arc additive manufacturing technique—A review. *J. Mater. Res. Technol.* **2021**, *13*, 754–768. [CrossRef]
27. Vázquez, L.; Rodríguez, N.; Rodríguez, I.; Alberdi, E.; Álvarez, P. Influence of interpass cooling conditions on microstructure and tensile properties of Ti-6Al-4V parts manufactured by WAAM. *Weld. World* **2020**, *64*, 1377–1388. [CrossRef]
28. Cunningham, C.R.; Flynn, J.M.; Shokrani, A.; Dhokia, V.; Newman, S.T. Strategies and processes for high quality wire arc additive manufacturing. *Addit. Manuf.* **2018**, *22*, 672–686. [CrossRef]

29. Köhler, M.; Fiebig, S.; Hensel, J.; Dilger, K. Wire and arc additive manufacturing of aluminum components. *Metals* **2019**, *9*, 608. [CrossRef]
30. Jafari, D.; Vaneker, T.H.J.; Gibson, I. Wire and arc additive manufacturing: Opportunities and challenges to control the quality and accuracy of manufactured parts. *Mater. Des.* **2021**, *202*, 109471. [CrossRef]
31. Baier, D.; Wolf, F.; Weckenmann, T.; Lehmann, M.; Zaeh, M.F. Thermal process monitoring and control for a near-net-shape Wire and Arc Additive Manufacturing. *Prod. Eng.* **2022**, *16*, 811–822. [CrossRef]
32. *ASTM E8/E8M-22*; Standard Test Methods for Tension Testing of Metallic Materials. 2022. Available online: https://www.astm.org/e0008_e0008m-22.html (accessed on 27 September 2023).[CrossRef]
33. Li, F.; Chen, S.; Shi, J.; Zhao, Y.; Tian, H. Thermoelectric cooling-aided bead geometry regulation in wire and arc-based additive manufacturing of thin-walled structures. *Appl. Sci.* **2018**, *8*, 207. [CrossRef]
34. Wu, B.; Ding, D.; Pan, Z.; Cuiuri, D.; Li, H.; Han, J.; Fei, Z. Effects of heat accumulation on the arc characteristics and metal transfer behavior in Wire Arc Additive Manufacturing of Ti6Al4V. *J. Mater. Process. Technol.* **2017**, *250*, 304–312. [CrossRef]
35. Gomes, B.F.; Morais, P.J.; Ferreira, V.; Pinto, M.; De Almeida, L.H. Wire-arc additive manufacturing of Al-Mg alloy using CMT and PMC technologies. *MATEC Web Conf.* **2018**, *233*, 31. [CrossRef]

Disclaimer/Publisher's Note: The statements, opinions and data contained in all publications are solely those of the individual author(s) and contributor(s) and not of MDPI and/or the editor(s). MDPI and/or the editor(s) disclaim responsibility for any injury to people or property resulting from any ideas, methods, instructions or products referred to in the content.